THE JOURNAL OF BIOLOGICAL CHEMISTRY
Vol. 279, No. 8, Issue of February 20, pp. 6893–6904, 2004
Printed in U.S.A.

SK3-1C, a Dominant-negative Suppressor of SK_{Ca} and IK_{Ca} Channels*

Received for publication, October 27, 2003, and in revised form, November 20, 2003
Published, JBC Papers in Press, November 24, 2003, DOI 10.1074/jbc.M311725200

Aaron Kolski-Andreaco‡§, Hiroaki Tomita¶, Vikram G. Shakkottai‡‖, George A. Gutman, Michael D. Cahalan‡, J. Jay Gargus‡ ‡‡, and K. George Chandy‡§§**

*From the Departments of ‡Physiology and Biophysics, ¶Psychiatry and Human Behavior, **Microbiology and Molecular Genetics, and ‡‡Pediatrics, University of California Irvine, Irvine, California 92697*

Small conductance Ca^{2+}-activated K^+ channels, products of the SK1-SK3 genes, regulate membrane excitability both within and outside the nervous system. We report the characterization of a SK3 variant (SK3-1C) that differs from SK3 by utilizing an alternative first exon (exon 1C) in place of exon 1A used by SK3, but is otherwise identical to SK3. Quantitative RT-PCR detected abundant expression of SK3-1C transcripts in human lymphoid tissues, skeletal muscle, trachea, and salivary gland but not the nervous system. SK3-1C did not produce functional channels when expressed alone in mammalian cells, but suppressed SK1, SK2, SK3, and IKCa1 channels, but not BK_{Ca} or K_V channels. Confocal microscopy revealed that SK3-1C sequestered SK3 protein intracellularly. Dominant-inhibitory activity of SK3-1C was not due to a nonspecific calmodulin sponge effect since overexpression of calmodulin did not reverse SK3-1C-mediated intracellular trapping of SK3 protein, and calmodulin-Ca^{2+}-dependent inactivation of Ca_V channels was not affected by SK3-1C overexpression. Deletion analysis identified a dominant-inhibitory segment in the SK3-1C C terminus that resembles tetramerization-coiled-coiled domains reported to enhance tetramer stability and selectivity of multimerization of many K^+ channels. SK3-1C may therefore suppress calmodulin-gated SK_{Ca}/IK_{Ca} channels by trapping these channel proteins intracellularly via subunit interactions mediated by the dominant-inhibitory segment and thereby reduce functional channel expression on the cell surface. Such family-wide dominant-negative suppression by SK3-1C provides a powerful mechanism to titrate membrane excitability and is a useful approach to define the functional *in vivo* role of these channels in diverse tissues by their targeted silencing.

Small conductance Ca^{2+}-activated K^+ channels (SK_{Ca})[1] tightly couple calcium signaling and regulation of membrane excitability in excitable cells and influence membrane potential in non-excitable cells (1–6). Three closely related genes, *SK1*, *SK2*, and *SK3*, known also as *K_{Ca}3.1–3.3*, *KCNN1-KCNN3*, and *SKCa1-SKCa3*, encode SK_{Ca} proteins (7–9). Functional SK_{Ca} channels are formed from the homo- or heterotetrameric association of SK1-SK3 products, use calmodulin (CaM) as a Ca^{2+} sensor, and are potently blocked by apamin, a peptide from bee venom (7, 8, 10, 11, 12). SK_{Ca} channels underlie the medium after-hyperpolarization current in neurons, a necessary component of the action potential that regulates firing frequency, and they modulate action potential threshold in skeletal muscle (2). SK_{Ca} channels in human Jurkat T cells play an important role in Ca^{2+} signaling (5).

Expression of SK3 has been reported in the brain, skeletal muscle, endothelium, uterus, and hepatobiliary cells (6, 7, 13–15). Recent quantitative RT-PCR studies have identified SK3 transcripts in other human tissues including the trachea, thyroid, spleen, and thymus (16). In the brain, SK3 is restricted to the midbrain monoaminergic neurons, basal ganglia, and limbic system, showing little overlap with SK1 and SK2 (7, 13, 14, 16, 17), and recent immunohistochemical studies have localized SK3 to presynaptic nerve termini (18). The SK3 channel serves as the intrinsic pacemaker in dopaminergic neurons and its pharmacological blockade leads to bursting action potentials and increased dopamine release (4, 19–21). In endothelium, SK3 has been reported to contribute to membrane hyperpolarization mediated by the endothelium-derived hyperpolarization factor, which is necessary for vasodilation (15). The channel has also been suggested to regulate membrane K^+ permeability of hepatobiliary cells following liver injury (6). Several lines of evidence have implicated SK3 in schizophrenia (9, 22–27), but these results are controversial because other studies have failed to confirm this disease association (28–35). SK3 has also been associated with anorexia nervosa (36), and dominant cerebellar ataxia (37), and has been reported to underlie the hyperexcitability associated with skeletal muscle denervation (2, 38).

Two SK3 variants with dominant-inhibitory activity have been reported. The first, SK3-Δ, is a frameshift mutant identified in a patient with schizophrenia (22, 24), and transcripts of the second, SK3-1B, have been detected in human (16), primate (accession no. BQ807391), porcine (BI341958), and bovine (CB467440) brain. When expressed in heterologous mammalian expression systems, both SK3-Δ and SK3-1B suppress SK1, SK2, and SK3 channels (16, 22). Such dominant-negative

* This work was supported by grants from the National Institutes of Health (MH59222), Rockefeller Brothers Fund (to K. G. C.), and National Ataxia Foundation (to K. G. C.). The costs of publication of this article were defrayed in part by the payment of page charges. This article must therefore be hereby marked "*advertisement*" in accordance with 18 U.S.C. Section 1734 solely to indicate this fact.

The nucleotide sequence(s) reported in this paper has been submitted to the GenBank™/EBI Data Bank with accession number(s) AF438203.

§ Supported by a National Institutes of Health predoctoral training grant in cellular and molecular neuroscience (1T32 N507444).

‖ Supported by a predoctoral fellowship from the American Heart Association Western States Affiliate.

§§ To whom correspondence should be addressed: Dept. of Physiology and Biophysics, Room 291, Joan Irvine Smith Hall, College of Medicine, University of California, Irvine, CA 92697. Tel.: 949-824-2133; Fax: 949-824-3143; E-mail: gchandy@uci.edu.

[1] The abbreviations used are: SK_{Ca}, small conductance Ca^{2+}-activated K^+ channel; IK_{Ca}, intermediate-conductance Ca^{2+}-activated K^+ channel; BK_{Ca}, large-conductance Ca^{2+}-activated K^+ channel; DIS, dominant-inhibitory segment; CaM, calmodulin; CaMBD: calmodulin-binding-domain; K_V, voltage-gated K^+ channel; Ca_V, voltage-gated Ca^{2+} channel; DMEM, Dulbecco's modified Eagle's medium; RACE, rapid amplification of cDNA ends; GFP, green fluorescent protein; IRES, internal ribosome entry site; ANOVA, analysis of variance; S, siemens.

behavior in the brain should have consequences similar to pharmacological blockade of SK_{Ca} channels, namely enhanced firing frequency and increased neurotransmitter release (3, 4, 7, 19–21).

Here we describe a new SK3 transcript, SK3-1C, that is expressed in peripheral human tissues but not the brain. When expressed heterologously in mammalian cells, SK3-1C suppressed SK1, SK2, SK3, and IKCa1 channels but not K_V or BK_{Ca} channels. Variations in the levels of functional SK_{Ca} and IK_{Ca} channels *versus* SK3-1C subunits in peripheral tissues may provide an endogenous mechanism to regulate membrane potential and Ca^{2+} signaling.

MATERIALS AND METHODS

5′-RACE—The sequence of the SK3-1C cDNA was extended by 5′-RACE (rapid amplification of cDNA ends) with an AP1 primer (Clontech, Palo Alto, CA) and a SK3-1C specific primer (5′-CTGTCCTTGCAGATGTCGCGTGGCAGGC-3′), using human adult Marathon-ready™ cDNA from human lymph node tissue (Clontech) as the template. Subsequently, a nested PCR was carried out using the RACE product and an SK3-1C-specific primer (5′-CAGCAAGCTCTAAGGAGTAGGTGCCAGC-3′) and an AP2 primer (Clontech). The longest product (206 bp) was purified using a QIAQuick™ gel extraction kit, ligated into PCR 2.1 vector and sequenced.

Real-time Quantitative RT-PCR—Human total RNA master panel (Clontech) and total RNA isolated from human lymph node tissue and peripheral blood lymphocytes were used to profile the expression pattern of SK3, SK3-1C, and IKCa1 with methods previously described (16). Following DNase digestion, total RNA (2 μg) was used as a template for first-strand cDNA synthesis using random hexamers (TaqMan™ reverse transcription reagents, Applied Biosystems). The mRNA for each SK3 transcript was measured by real-time quantitative RT-PCR using a Prism model 7000-sequence detection instrument (PE Applied Biosystems). Forward and reverse primers and TaqMan™ fluorescent probes were designed by Primer Express version 1.5 (Applied Biosystems). The sequences of forward primers, designed to anneal to exon 1, were 5′-GCGACATCTGCAAGGACAGTT-3′ for SK3-1C, and 5′-GGAACTGGCATTGGACTCATG-3′ for IKCa1. The reverse primers, designed to anneal to exon 2, were 5′-CAACGAAAACATGGAGTCCTTTATAG-3′ for SK3-1C, and 5′-TGCTGATCGTGCATTTAACCA-3′ for IKCa1. The TaqMan™ fluorescent probes (5′-labeled with 6FAM, and 3′-labeled with TAMRA as a quencher), designed to anneal to sequences between the forward and reverse primers, were 5′-TTTGGTGTTTTGCTTCAGGTTATAGATGGAGAGA-3′ for SK3-1C, and 5′-TGCTCGTGGGCGCTCTACCTGTTC-3′ for IKCa1. The SK3-1C and IKCa1 amplification products were 83 and 100 bp, respectively. The threshold cycle, C_t, which correlates inversely with the target mRNA levels, was measured as the cycle number at which the reporter fluorescent emission increased above a pre-set threshold level. To obtain absolute quantification, standard curves were plotted for every assay and were generated using defined concentrations of SK3-1C in Image clone 3678178, and IKCa1 cDNA cloned into the eGFPN1 vector. Standard curves for each amplicon were plotted from 8 different concentrations of standards, each run in triplicate. Concentrations were determined by spectrophotometry and purity confirmed by agarose gel electrophoresis. Purified clones were diluted to eight different concentrations and stored in single-use aliquots at −20 °C and the same diluted preparations were used throughout.

Cell Culture and Transfection—All cells were kept in a 37 °C humidified incubator with 5% CO_2 and were split 1:10 twice a week. Unless otherwise stated, all reagents used in tissue culture were obtained from Sigma. Rat pheochromocytoma PC12 cells were maintained in Dulbecco's Modified Eagle Medium (DMEM) supplemented with 10% horse serum, 5% fetal calf serum, and 2 mM glutamine-penicillin-streptomycin. HEK293T cell lines stably expressing human SK1, rat SK2, and human IKCa1 were a generous gift from Dr. Khaled Houamed (University of Chicago), and were kept in DMEM, 10% fetal calf serum, and 2 mM glutamine-penicillin-streptomycin. Puromycin (10 μg/μl) was used as a selection marker to preserve channel expression. The HEK293T cell line that stably expresses human BK_{Ca} was a generous gift from Dr. Andrew Tinker (University College London). The HEK293T cell line that stably expresses the cloned L-type Ca_V channel ($Ca_V1.2b$ + $\beta 2$ α) was a gift from Dr. Franz Hofmann (Institut für Pharmakologie und Toxikologie, Munich, Germany). This cell line was grown in DMEM, supplemented with 10% dialyzed fetal calf serum, and 2 mM glutamine-penicillin-streptomycin, with selection markers G418 (20 μg/ml), and hygromycin B (50 μg/ml) to preserve channel expression.

All constructs were transfected using the FuGENE 6 transfection reagent (Roche Applied Science). Cells were seeded at a density of 200,000–300,000/well in a 12-well plate and were grown overnight. Transfection complexes consisting of 3 μl of FuGENE 6 and 2 μg of DNA were incubated in serum-free Optimem (Invitrogen, Life Technologies, Inc.) for at least 20 min before application to cells. Electrophysiology and confocal imaging were performed 72-h post-transfection.

Generation of Constructs—SK3-1C and all its deletion constructs were engineered into the IRES-EGFP vector (Clontech), using 5′ HindIII and 3′ BamHI restriction sites. PCR reactions were catalyzed by thermalase DNA polymerase (Invitrogen), and the incorporation of stop codons in the 3′-primer generated 4 SK3-1C deletion mutants. The two SK3 C-terminal fragment constructs were generated through a PCR reaction amplifying a region beginning with an internal methionine (M330) artificially placed in a good Kozak consensus sequence. One of these C-terminal constructs was placed in the IRES-EGFP vector, and the other was made into a GFP fusion protein by cloning it into the eGFP-N1 plasmid (Clontech). CaM, a generous gift from Dr. Mitsuhiko Ikura (University of Toronto), was inserted into the first multiple cloning site of the bicistronic pIRES vector (Clontech) directly 3′ to the CMV promoter using NheI and EcoRI restriction sites. Inserted at SalI and NotI sites, directly downstream to the IRES element, was a C-terminally tagged SK3-1C-EGFP fusion construct, which yielded a bicistronic expression construct, CaM-IRES-SK3-1C-EGFP, which produced both CaM and SK3-1C-eGFP driven by the same CMV promoter. All constructs were sequenced and shown to contain the expected open reading frames.

Whole Cell Recording—Whole cell patch-clamp recordings for SK_{Ca}, IK_{Ca}, BK_{Ca}, and K_V currents were performed using a 1μM free Ca^{2+} internal pipette solution containing (in mM): 145 K^+ aspartate, 8.5 $CaCl_2$, 10 EGTA, 10 HEPES, and 2 $MgCl_2$ (pH 7.4; 300 mosM). When recording from stably transfected HEK cells, a sodium aspartate Ringer solution comprised of (in mM) 155 Na^+ aspartate, 4.5 KCl, 2 $CaCl_2$, 1 $MgCl_2$, and 10 HEPES (pH 7.4; 300 mosM) was used as a bath solution. A 160 mM K^+ aspartate solution was used when recording SK_{Ca} currents from PC12 cells, which contained (in mM): 10 HEPES, 2 $CaCl_2$, and 1 $MgCl_2$ (pH 7.4; 300 mosM). Glass patch-clamp electrodes (Kimble) with pipette resistances ranging from 1.8–2.5 MΩ were used to form gigaohm seals. Recordings were made using an EPC-9 amplifier and Pulse software (HEKA Instruments). In voltage-clamp experiments, cells were held at −80 mV, and SK_{Ca} and IK_{Ca} currents were recorded using voltage ramps from −120 to 40 mV (80 mV for BK_{Ca}) in 200 ms. Slope conductances were analyzed between −70 to −50 mV from cells in which the series resistance was less than 10 MΩ. Prior to recording, cells were placed on coverslips coated with polylysine and were allowed to adhere for at least 15 min.

Whole cell recording for $Ca_V1.2$ currents in stably transfected HEK293T cells were performed using an internal solution containing (in mM): 102 CsCl, 10 TEA Cl, 10 EGTA, 5 HEPES, 3 Na_2ATP, and 1 $MgCl_2$ (pH 7.4; 300 mosM). Bath solutions contained (in mM) either 30 $BaCl_2$ or 20 $CaCl_2$, 82 NaCl, 5.4 CsCl, 10 TEA Cl, 5 HEPES, and 10 glucose (pH 7.4; 300 mosM). In PC12 cells, whole cell recording for Ca_V currents was performed using an internal solution containing (in mM): 150 CsCl, 1 EGTA, 10 HEPES, 2 MgATP, and 0.5 GTP (pH 7.2; 300 mosM). External solutions contained (in mM) either 20 $BaCl_2$ or 20 $CaCl_2$, 135 TEA Cl, 4 KCl, 1 $MgCl_2$ and 10 HEPES (pH 7.2; 300 mosM). Using a holding potential of −80 mV, families of Ca_V currents were elicited by 600-ms pulses from −40 to 40 mV given at 10 s intervals. Mock- and SK3-1C-IRES-GFP-transfected PC12 cells were plated onto coverslips and grown for 72 h in nerve growth factor-containing medium prior to recording.

Immunostaining—Prior to immunostaining, transfected PC12 cells were plated onto glass coverslips and allowed to settle overnight. Cells were washed with phosphate-buffered saline for 5 min, fixed with 4% paraformaldehyde in phosphate-buffered saline for 20 min, and permeablilized with Triton X-100 for 20 min. Cells were then washed three times with phosphate-buffered saline for 5 min, both before and after a 4-hr incubation with the anti-SK3-specific antibody that reacts with the N terminus of full-length SK3 (Alomone Labs), and following a 1-h incubation with the secondary Alexa-594-conjugated goat-anti-rabbit Ig antibody (Molecular Probes). Antibodies specific for the C termini of rodent SK3 were gifts from Dr. Hans-Gunther Knaus (Innsbruck, Austria) (17) and Dr. Martin Stocker (University College London).

Confocal Microscopy and Image Analysis—An MRC-1024 laser-scanning confocal microscope (BioRad) was used to acquire images. The microscope was housed on an inverted Nikon Diaphot 200 stand, and 1-μm sections of PC12 cells were obtained using a ×100 oil immersion objective. Excitation wavelengths of 488 and 568 nm were used to

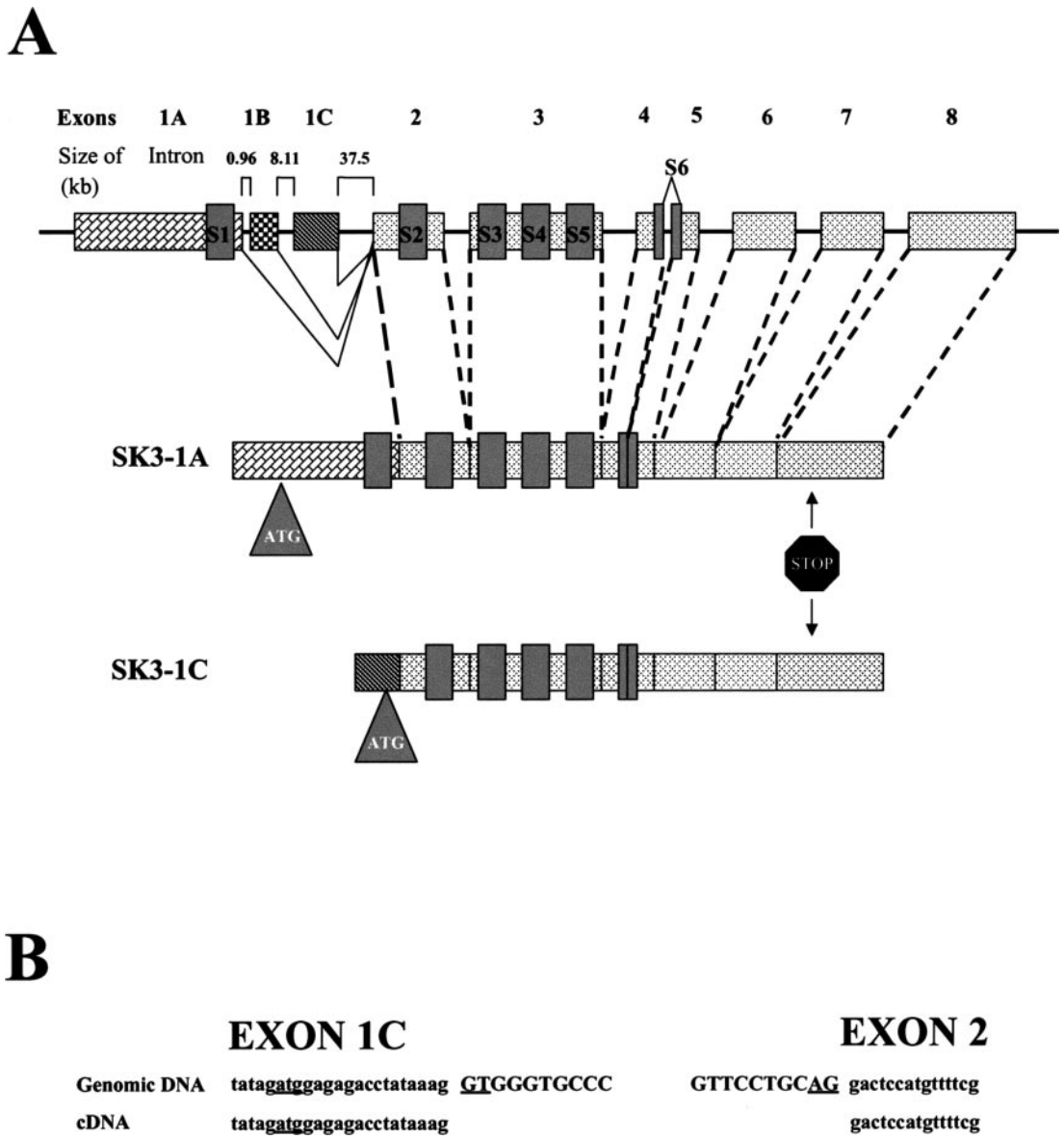

FIG. 1. **Genomic organization of SK3 and SK3-1C.** *A*, schematic representation of the intron-exon organization of the SK3 locus and SK3 and SK3-1C cDNA. *Solid lines* show the splicing events occurring at the junction between exons 1A and 1C with exon 2. The lengths of the first three introns are given in kb. *B*, 5′- and 3′-boundaries of the intron that lies between exon 1C and exon 2. The splice donor consensus sequences are *underlined* as well as the first putative initiation codon.

visualize GFP and Alexa-594 fluorescence respectively, and images were collected with 522/35 and 605/32 emission filters. Confocal Assistant and Adobe Photoshop were used to process confocal sections, and pixel intensities of fluorescence histograms representative of the localization of tagged SK3 were computed using the Scion Image 4.0.2 software. The image of each cell was bisected in each of three axes. Pixel intensity was determined and averaged along each of these axes. The borders of an individual cell were defined as a rise in pixel intensity 50% above background levels. The length of all pixel intensity histograms was scaled to an arbitrarily chosen histogram, and the numerical pixel intensity values were averaged for SK3-1C-IRES-GFP-, IRES-GFP-, and mock-transfected cells in all axes, in order to generate an average line plot histogram for the entire experimental group. A ratio of presumed membrane to intracellular fluorescence was calculated by partitioning the line plot histogram into three sections, averaging the two outer thirds (cell periphery), and dividing that average by the area underneath the central portion (cell interior).

RESULTS

Identification of a Novel Truncated SK3 Isoform, SK3-1C—Multiple ESTs encoding a novel isoform of SK3 were discovered during a BLAST search of GenBank™ with the human SK3 sequence (AJ251016). These ESTs were derived primarily from Burkitt's lymphoma (accession nos: AL560989, BE397619, BE562092, BE513322, BE397440) and lymphoid tissues including germinal center B cells (AA490752, AW499701, AA284005, AA256031) and spleen (BQ710272). By sequencing the entire insert of IMAGE clones 686525, 700710, 824081, corresponding to ESTs AA256031, AA284005, AA490752, and by 5′-RACE to define the approximate transcription start site, we determined the composite 1921 bp sequence of this new isoform we term SK3-1C. The SK3-1C sequence has been deposited in GenBank™ (accession no. AF438203).

Alignment of the SK3-1C cDNA sequence with the published sequence of the SK3 genomic locus (AF336797) revealed the intron-exon organization of SK3-1C (Fig. 1*A*). SK3-1C, SK3, and the recently described SK3-1B isoform all utilize exons 2–8 and differ only in the usage of three first exons: exon 1A by SK3, exon 1B by SK3-1B, and exon 1C by SK3-1C. Exon 1C encodes the 5′-non-coding sequence of the SK3-1C transcript (first 146 bp) and lies ~8.1-kb downstream to exon 1B, which is located 0.7 kb 3′ to exon 1A. The splice donor and acceptor sites flanking the intron between exons 1C and 2 are shown in Fig.

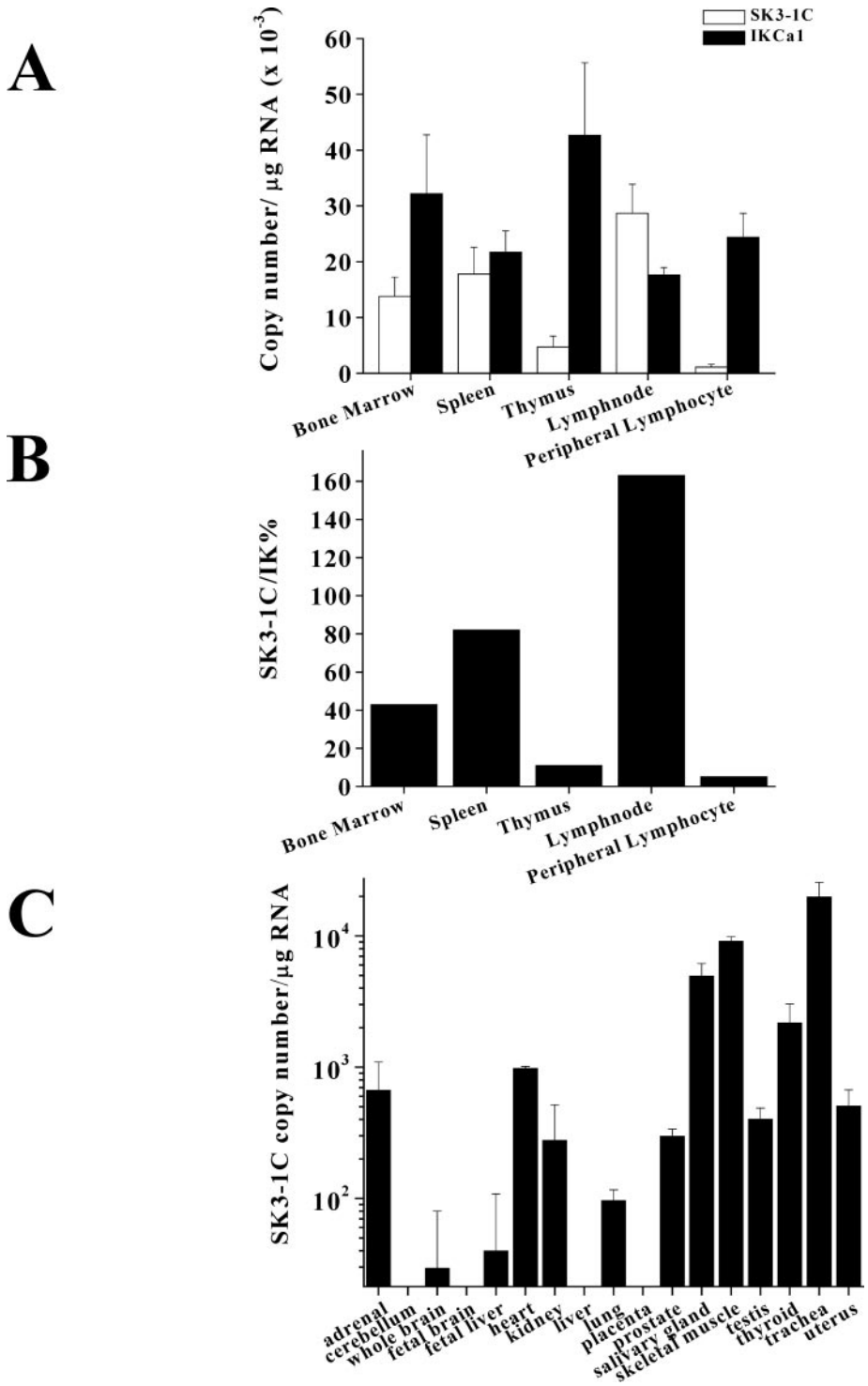

FIG. 2. **Distribution of SK3-1C transcripts in human tissues determined by Taqman™ quantitative RT-PCR.** *A*, SK3-1C and IKCa1 copy number/μg RNA in lymphoid tissues is shown in this bar graph with *error bars* representing S.E. *B*, SK3-1C/IKCa1 ratio in lymphoid tissues. *C*, SK3-1C copy number/μg RNA in human non-lymphoid tissues.

1*B*. Interestingly, a BLAST search with the exon 1C sequence does not detect a match in the completed rat and mouse genomes. Since the sequences of 5′-non-coding regions tend to diverge between species, our inability to identify a matching sequence does not necessarily exclude the presence of an SK3-1C-like transcript in rodents.

SK3-1C Transcripts Are Present in Human Hematopoietic and Muscle Tissues but Not the Brain—Quantitative real time RT-PCR (TaqMan™) was utilized to measure SK3-1C transcript levels in various human tissues. We initially focused on hematopoetic tissues because all the SK3-1C ESTs had a lymphoid origin. Abundant levels of SK3-1C (>10,000 copies/μg RNA) were detected in bone marrow, spleen and lymph node, and lower levels in the thymus and peripheral blood leukocytes (Fig. 2*A*). Since the predominant Ca^{2+}-activated K^+ channel in lymphoid tissues is IKCa1 (5, 39) we compared transcript levels for this channel (Fig. 2*A*) with those found for SK3-1C. The ratio of SK3-1C/IKCa1 was highest in the lymph node, followed by the spleen, bone marrow, thymus, and peripheral blood leukocytes (Fig. 2*B*).

Analysis of a larger panel of tissues revealed negligible expression (< 500–1000 copies/μg RNA) of SK3-1C mRNAs in whole brain, fetal brain, and cerebellum (Fig. 2*C*), tissues known to abundantly express SK3 and SK3-1B (15). However, abundant expression of SK3-1C was detected in trachea, and lower levels in skeletal muscle, salivary gland,

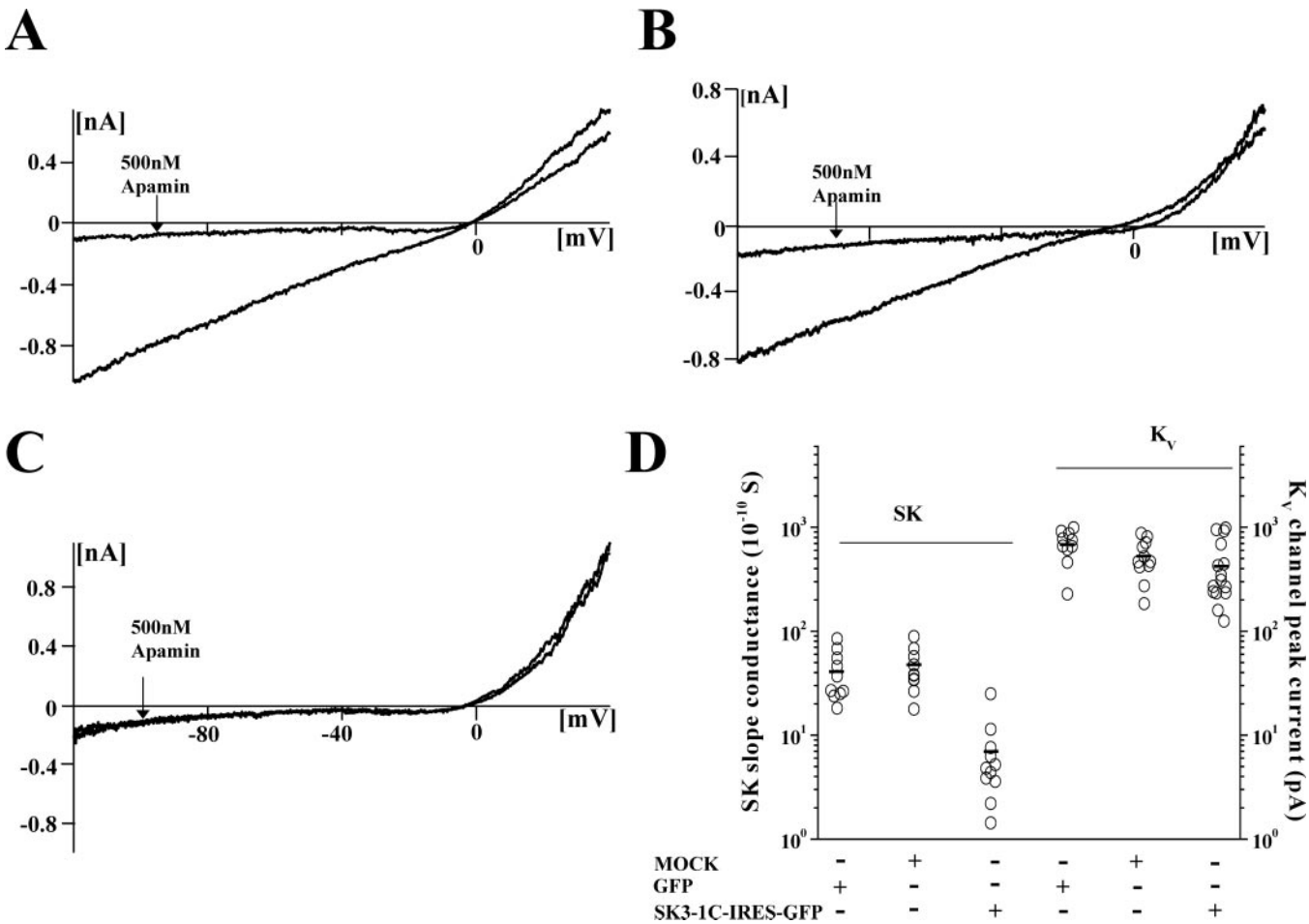

FIG. 3. **Dominant-negative suppression of endogenous SK_{Ca} currents in PC12 cells by SK3-1C.** *A*, representative trace of inward SK_{Ca} current completely blocked by 500 nM apamin leaving a residual apamin-insensitive K_V current at positive potentials. Recordings were performed in a symmetric K^+ solution, hence the reversal potential is zero. Whole cell channel activity was monitored via 200 ms voltage ramps from −120 to 40 mV with 1 μM free Ca^{2+} in the internal solution. *B*, representative control trace showing that SK_{Ca} currents are unaffected by the expression of the IRES-GFP vector. *C*, SK3-1C-IRES-GFP transfection causes significant attenuation of apamin sensitive SK_{Ca} currents, while the apamin-insensitive K_V component is unaffected. *D*, scatter plot showing the specificity of SK3-1C dominant-negative suppression for SK_{Ca} currents over native K_V currents in PC12 cells. SK3 slope conductance was significantly reduced in cells transfected with SK3-1C-IRES-GFP (mean ± S.E., 6.88 ± 1.98 S^{-10}; one-way ANOVA, $p < 0.00005$), but not mock-transfected cells or IRES-GFP-transfected cells (41.1 ± 6.97 S^{-10} and 46.1 ± 6.15 S^{-10}). On the other hand, native peak K_V currents were unaffected by SK3-1C-IRES-GFP expression (mean ± S.E., 440 ± 76.4 pA) and were comparable to those recorded in mock and IRES-GFP vector-transfected cells (692 ± 71.4 and 527 ± 64.6 pA, respectively; $p > 0.05$, one way ANOVA). *Black bars* indicate the mean for each group in the scatter plot.

thyroid gland, uterus, testis, prostate, heart, kidney, lung, and adrenal gland (Fig. 2*C*). The levels of SK3-1C in the trachea and salivary gland are higher than that reported for SK3, but in other non-neuronal tissues the levels of SK3-1C are comparable to that for SK3 (16). Thus, SK3-1C is natively expressed in peripheral human tissues but not brain. The lack of an antibody specific for the shared C-terminal region present in human SK3 and SK3-1C precluded attempts to identify SK3-1C protein in native human tissues. The two antibodies that recognize the C termini of rodent SK3 (see "Materials and Methods") do not cross-react with human SK3 or SK3-1C (data not shown).

Dominant-negative Suppression of Endogenous SK_{Ca} Currents in PC12 Cells by SK3-1C—Many other non-functional ion channel isoforms encoded by naturally occurring transcripts (KCNQ1-b, KCNQ2–1b, SK3-1B, tKvLQT1/KvLQT-2, KCNQ2S, $HERG_{USO}$, SloV1, Kv5.1, Kv6.1-Kv6.3, Kv8.1, Kv9.1, $Ca_V1.1$, $Ca_V2.2$) or by disease-associated mutant mRNAs (KCNQ1, KCNH2, Kv1.1, SK3-Δ) have not been proven to exist as proteins in native tissues (7, 16, 22, 40–49). However, experiments in heterologous expression systems have shown them to act as specific dominant-negative suppressors of their functional counterparts (7, 16, 22, 42, 45–48). Since SK3-1C did not produce functional channels when expressed heterologously in mammalian cells (data not shown), we used the approach described for other non-functional K^+ channel isoforms to ascertain whether SK3-1C exhibits dominant-inhibitory activity.

The complete coding sequence of SK3-1C was engineered into a bicistronic construct (IRES-EGFP) that independently expressed GFP through an IRES element. The SK3-1C-IRES-GFP construct was transfected into PC12 cells, which endogenously express apamin-sensitive SK3 currents (16). Whole-cell patch-clamp recordings using 200-ms ramps from −120 to 40 mV were performed to assess the level of SK_{Ca} current. Under symmetric K^+ conditions in mock-transfected cells, apamin-sensitive SK_{Ca} currents were inward at negative potentials, reversed at 0 mV and showed little rectification (Fig. 3*A*). At positive potentials, a voltage-gated apamin-insensitive K_V component was also present (Fig. 3*A*), which served as an internal control to demonstrate the specificity of the SK3-1C dominant-inhibitory activity. Transfection of the SK3-1C-IRES-GFP construct completely abolished the apamin-sensitive SK_{Ca} component without affecting the apamin-insensitive

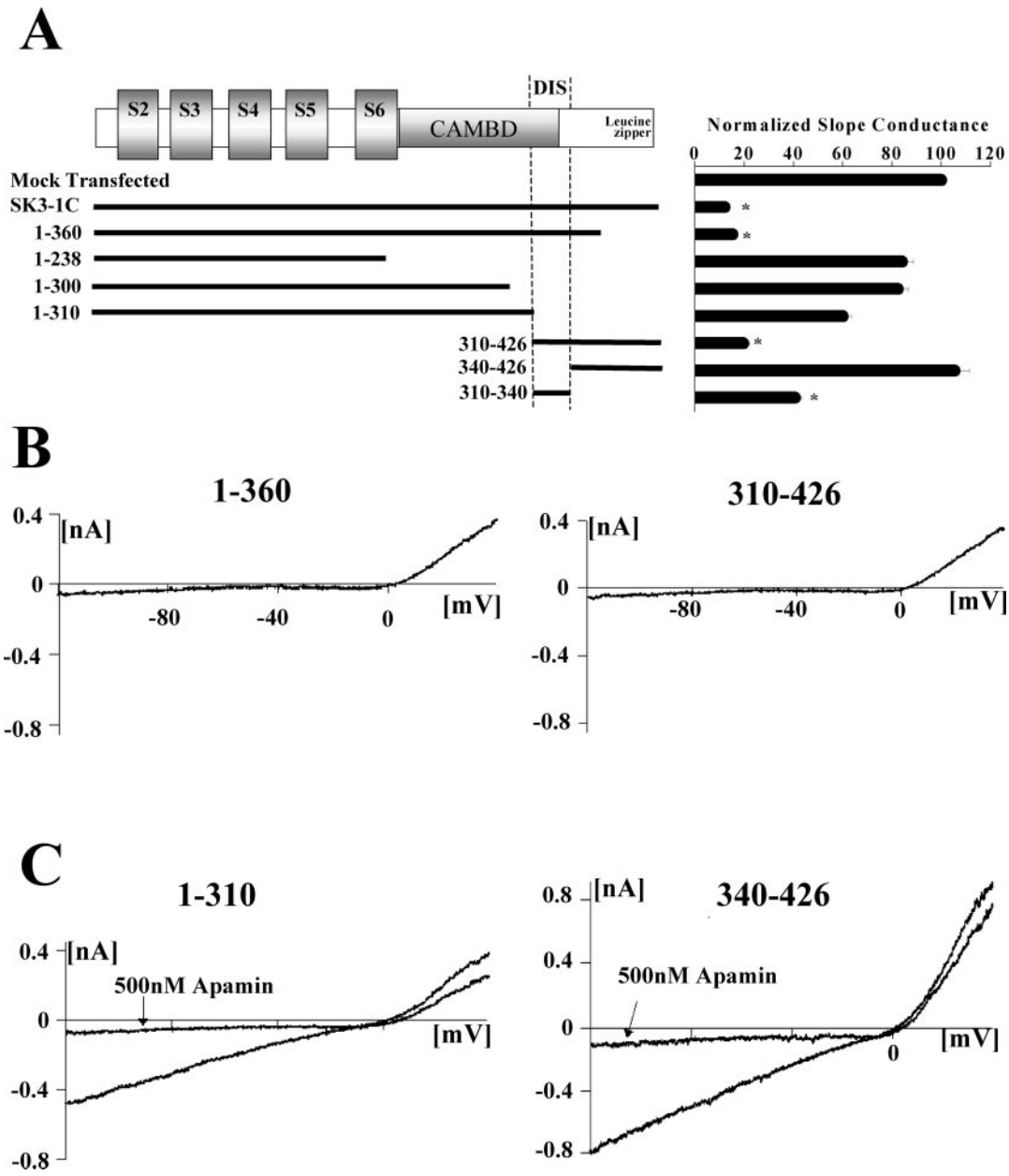

FIG. 4. **Deletion analysis reveals a critical region necessary for dominant-negative suppression of SK3 currents in PC12 cells.** Recording conditions are as stated in Fig. 3. *A*, schematic displaying each of the deletions tested. The bar graph on the right shows the normalized slope conductance values for SK_{Ca} currents following transfection of each deletion construct. Fragments 1–360 (15.25 ± 1.037, $n = 8$, one-way ANOVA, $p < 0.000001$), 310–426 (19.65 ± 2.751, $n = 12$; one-way ANOVA, $p < 0.000001$), and 340–426 (40.69 ± 2.76692: one-way ANOVA, $p < 0.000001$) show an appreciable degree of suppression. The remaining constructs lacked dominant inhibitory activity, yielding slope conductance values (1–238: 84.22 ± 4.547, $n = 9$, 1–300: 82.5 ± 4.125, $n = 10$, 1–310: 60.125 ± 3.42713, $n = 10$, 340–426: 105.5 ± 5.8025) close to those exhibited by controls. *B*, representative *traces* showing that fragments 1–360 and 310–426 retain dominant-inhibitory activity. *C*, representative *traces* showing that fragments 1–310 and 340–426 lack suppressive ability.

K_v component (Fig. 3*C*). We controlled for nonspecific effects of heterologous expression by demonstrating that SK_{Ca} and K_V currents in cells transfected with the IRES-EGFP vector were identical to those in mock-transfected cells (Fig. 3*B*).

The scatter plot in Fig. 3*D* demonstrates the selective ability of SK3-1C to suppress SK_{Ca} currents without affecting K_V currents. SK_{Ca} slope conductance was significantly reduced in SK3-1C-IRES-GFP-transfected cells (mean ± S.E., 6.88 ± 1.98 nS; one-way ANOVA $p < 0.00005$), when compared with mock- (41.1 ± 6.97 nS) or IRES-EGFP-transfected cells (46.1 ± 6.15 nS). In contrast, the peak K_V current in SK3-1C-transfected PC12 cells (mean ± S.E., 440 ± 76.4 pA) was comparable to that in mock- and IRES-EGFP vector-transfected cells (692 ± 71.4 and 527 ± 64.6 pA respectively; $p > 0.05$, one-way ANOVA). These data demonstrate that SK3-1C specifically suppresses endogenous SK_{Ca} currents in PC12 cells in a dominant-negative manner.

```
hSK3/SK3-1C  MEQRKLSDQANTLVDLSKMQNVMYDLITEL
hSK1         IEQGKLNDQANTLTDLAKTQTVMYDLVSEL
hSK2         MEQRKLNDQANTLVDLAKTQNIMYDMISDL
hIKca1       LKHRKLREQVNSMVDISKMHMILYDLQQNL
```

FIG. 5. **Alignment of the SK3-1A/1B/1C DIS sequence with corresponding regions in SK1, SK2, and IKCa1.** Residues identical in all four channels are highlighted in *bold*. *Underlined* residues are similar in hydrophobicity, polarity, charge, or size when compared with SK3.

A Conserved C-terminal Domain in SK3-1C Is Critical for Dominant-negative Suppression—Deletion analysis identified

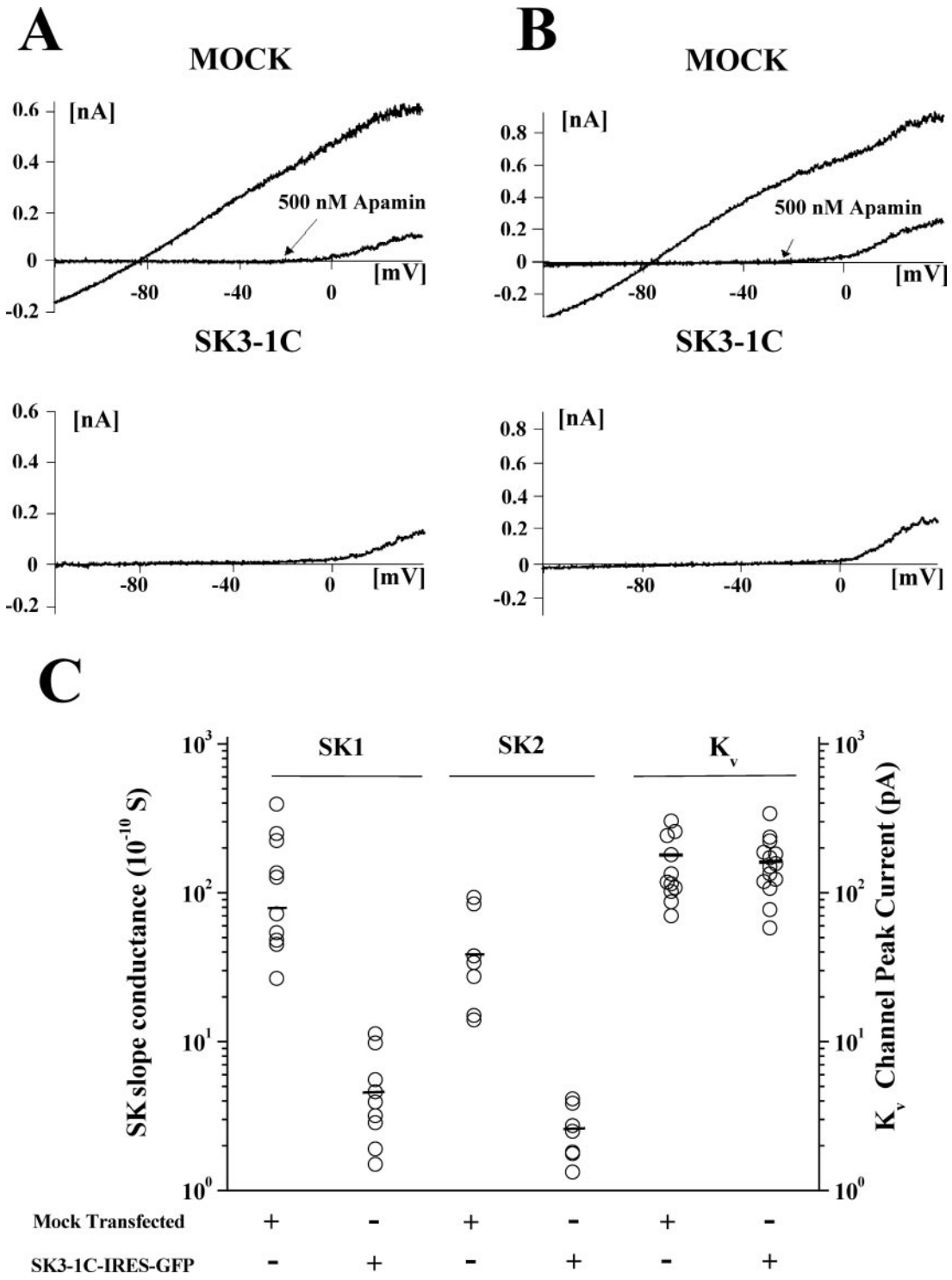

FIG. 6. **Cross-channel suppression by SK3-1C of SK1 and SK2 channels in HEK-293T cells.** Recording conditions are as stated in Fig. 3. *A*, apamin-sensitive SK1 current in a mock-transfected cell (*top*), and SK3-1C-IRES-GFP suppresses SK1 current (*bottom*). Note that the K_V current activated at more positive potentials is unaffected. *B*, apamin-sensitive SK2 current in a mock-trasnfected cell (*top*) and SK3-1C-IRES-GFP suppresses SK2 current (*bottom*). K_V current is unaffected. *C*, scatter plot comparing SK_{Ca} slope conductance and K_V peak current values for mock- and SK3-1C-transfected cells. SK3-1C dominant-negatively inhibited SK1 ($4.96 \pm 1.1\ S^{-10}$, $n = 9$, *versus* mock-transfected cells: $88.94 \pm 29.4\ S^{-10}$, $n = 7$ $p < 0.01$), and SK2 ($2.59 \pm 0.402\ S^{-10}$, $n = 7$ *versus* mock-transfected cells: $43.6 \pm 12.1\ S^{-10}$, $n = 7$, $p < 0.01$) channels. K_V peak currents were unaffected by SK3-1C (161 ± 19.4 pA, $n = 14$ *versus* mock-transfected cells: $176. \pm 25.4$ pA, $n = 14$). *Solid black bars* represent the mean values for each group.

a short region in the C terminus of SK3-1C that is required for dominant-negative inhibition of endogenous SK_{Ca} currents in PC12 cells. Dominant-inhibitory activity was retained by the 1–360 SK3-1C deletion mutant and by the 310–426 fragment that spans the C terminus of SK3-1C (Fig. 4, *A* and *B*). In contrast, deletion constructs 1–238, 1–300, 1–310, and 340–426 did not suppress SK_{Ca} currents in PC12 cells (Fig. 4, *A* and *C*). The *right panel* of Fig. 4*A* summarizes data from multiple cells (normalized to mock-transfected cells) and shows that the 1–360, 310–426, and 310–340 fragments, but not the other deletion fragments, suppress SK_{Ca} currents. These results identify the dominant-inhibitory segment (DIS) between 310

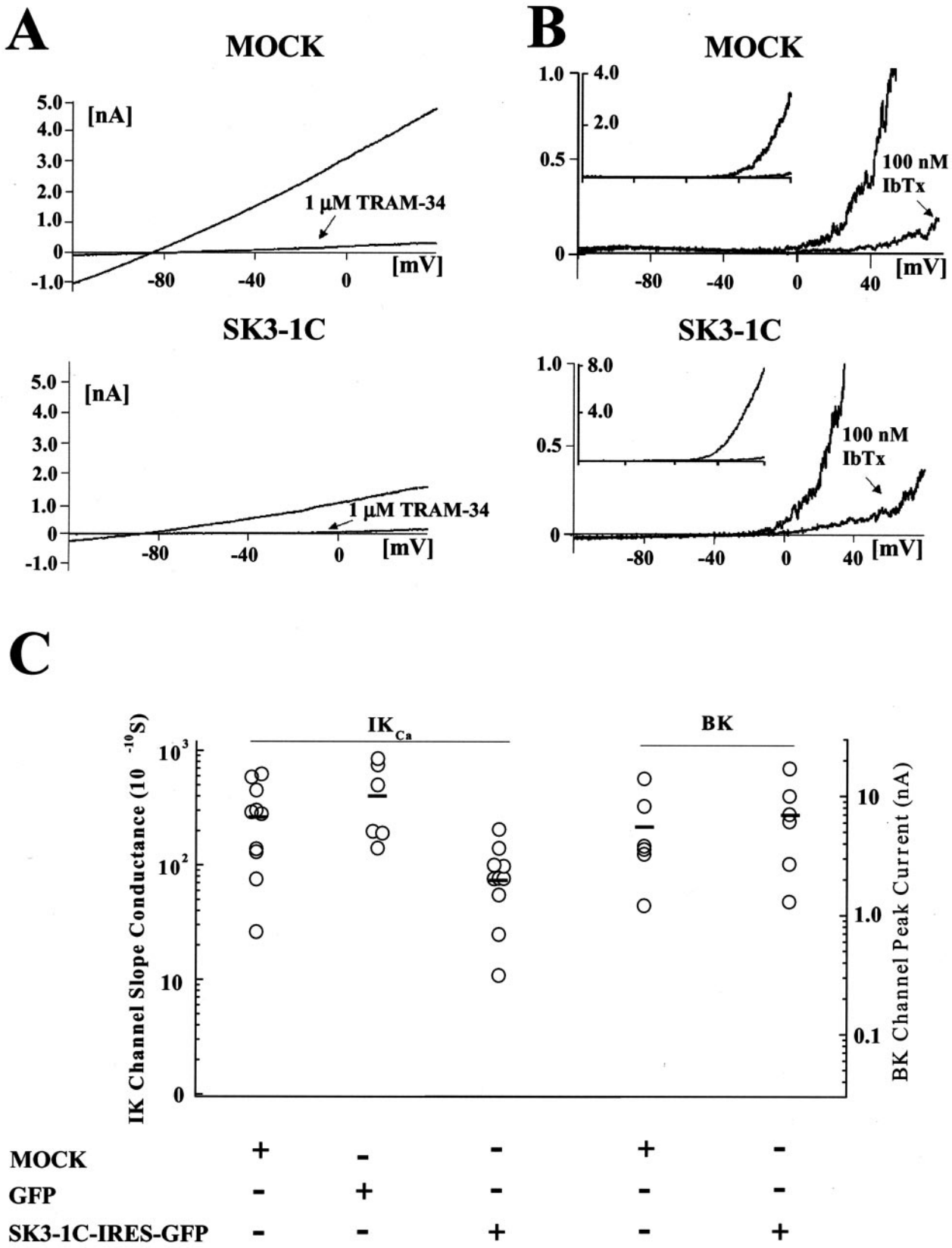

FIG. 7. **SK3-1C significantly reduces IKCa1 currents, but not BK_{Ca} currents.** Recording conditions are as stated in Fig. 3. *A*, TRAM-34-sensitive IKCa1 current in mock-transfected cell (*top*) and SK3-1C-IRES-GFP suppresses IKCa1 (*bottom*). *B*, iberitoxin (*IbTX*)-sensitive BK_{Ca} current in a mock-transfected cell (*top*) and SK3-1C-IRES-GFP-transfected cell (*bottom*); SK3-1C did not suppress the BK_{Ca} current. Note that the current magnitude is nearly twice as large in the *bottom trace* as that seen in the *control trace* above. Recording conditions were identical to that used for IKCa1 and the SK_{Ca} channels, however, for maximal activation a ramp from −120 to 80 mV was used. *C*, scatter-plot comparing whole cell IK_{Ca} slope conductance and BK_{Ca} peak current in mock- and SK3-1C-IRES-GFP-transfected cells. IKCa1 was suppressed by SK3-1C ($86.4 \pm 17.7\ S^{-10}$, $n = 10$) compared with mock ($289 \pm 65.5\ S^{-10}$, $n = 10$) and IRES2-eGFP-transfected cells ($437 \pm 126\ S^{-10}$, $p < 0.01$ one-way ANOVA) cells. There was no effect of SK3-1C on average BK_{Ca} peak current (7.3 ± 2.3 nA), as peak current values were similar to mock-transfected cells (5.6 ± 1.9 nA, $p > 0.5$, Student's *t* test).

and 340 as being necessary and sufficient for dominant-inhibitory activity of SK3-1C.

SK3-1C Suppresses SK1, SK2, SK3, and IKCa1 Currents but Not BK_{Ca}—The critical DIS domain is shared by SK3, SK3-1B, and SK3-1C, and shares ~70% sequence identity with the corresponding segments in SK1 and SK2 and 46% with the region in IKCa1 (Fig. 5). Most striking is the conservation of hydrophobic residues spaced ~3–4 residues apart, a characteristic of tetrameric-coiled-coil domains that contribute to tetramer stability in multimeric channels (50). This high degree of sequence similarity of the DIS and its resemblance to tetramerization-coiled-coiled domains suggests that SK3-1C might suppress SK1, SK2, and possibly IKCa1 currents in a dominant-negative fashion via DIS-mediated interactions. We tested this idea by evaluating the ability of SK3-1C to suppress SK1, SK2, and IKCa1 channels stably expressed in HEK-293T cells.

With 1 μM free Ca^{2+} in the pipette and under symmetric K^+ conditions, whole cell patch-clamp recordings using 200 ms ramp pulses from −120 to 40 mV revealed prominent apamin-sensitive SK1 and SK2 currents in mock-transfected cells (Fig. 6, *A* and *B*, *top panel*). The residual currents seen at positive potentials represent K_V channels in these cells. SK3-1C-IRES-GFP transfection completely abrogated SK1 and SK2 currents (Fig. 6, *A* and *B*, *bottom panels*). Analysis of multiple mock- and SK3-1C-IRES-GFP-transfected cells showed that SK3-1C reduced SK1 and SK2 current amplitude by more than an order of magnitude without affecting the K_V component (Fig. 6*C*). Whole cell recording under similar conditions revealed IKCa1 current in mock-transfected cells that were blocked by 1 μM TRAM-34, a specific inhibitor of the channel, and SK3-1C transfection significantly suppressed this IKCa1 current (Fig. 7*A*). An approximate 5-fold reduction in IK_{Ca} slope-conductance (86.4 ± 17.7 nS, $n = 10$) was evident in SK3-1C-transfected cells compared with mock- (289 ± 65.5 nS, $n = 10$) and IRES-eGFP vector-transfected (437 ± 126 S^{-10}, $p < 0.01$; one-way ANOVA) cells (Fig. 7*C*).

The distantly related iberiotoxin-sensitive BK_{Ca} channel (stably expressed in HEK-293 cells) was unperturbed by transfection of SK3-1C (Fig. 7, *B* and *C*), the peak current values in these cells (7.3 ± 2.3 nA) being similar to that in mock-transfected cells (5.6 ± 1.9 nA, $p > 0.01$; Student's t test). The selective suppression by SK3-1C of SK1, SK2, and IKCa1 suggests a powerful dominant-inhibitory mechanism by which this entire closely related SK_{Ca}/IK_{Ca} channel family might be regulated.

Dominant-negative Suppression by SK3-1C Is Associated with Intracellular Sequestration of SK3 Protein—To determine whether SK3-1C exerts its dominant-inhibitory effect in PC12 cells by altering the sub-cellular localization of the native SK3 protein, we visualized immunostained-SK3 using confocal microscopy. A transmitted light image of a mock-transfected PC12 cell is shown in Fig. 8*A* (*top panel*). Using an antibody specific for the N terminus of SK3 (that does not interact with SK3-1C) followed by an Alexa-594-conjugated secondary antibody, endogenous SK3 protein was found to have an annular pattern consistent with surface membrane expression (Fig. 8*A*, *middle panel*). Pixel intensity of presumptive membrane and intracellular SK3 fluorescence was discerned using Scion image software, and the histogram displaying average fluorescence intensity (*bottom panel*, Fig. 8*A*) showed two sharp peaks representing the annular distribution pattern. The annular distribution of SK3 was dramatically altered by the expression of SK3-1C, and intense staining was observed in the cytoplasm (Fig. 8*C*, *middle*). This change was reflected in the average fluorescence intensity histogram for SK3 (Fig. 8*C*, *bottom panel*), which shows a higher level of relative fluorescence in the center of the line plot than in mock- (Fig. 8*A*, *bottom*) or GFP-transfected (Fig. 8*B*, *bottom*) cells. These results, together with the electrophysiological data, suggest that the SK3-1C dominant-inhibitory activity is due to intracellular sequestration of SK_{Ca} proteins and the reduction of functional channels on the cell surface.

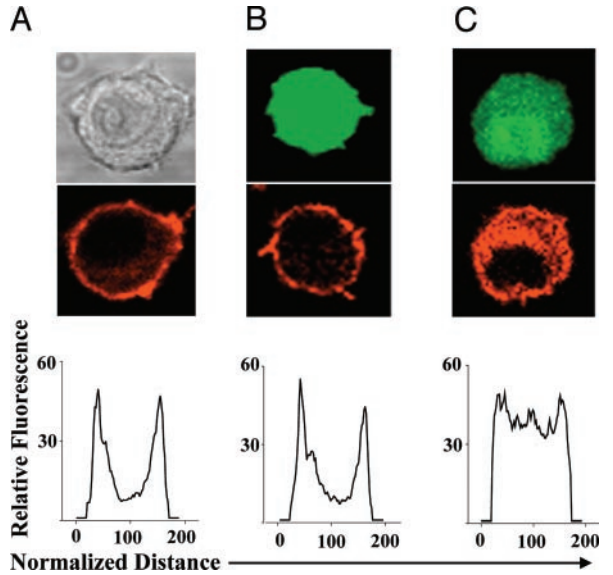

FIG. 8. **SK3-1C-IRES-GFP expression causes a change in localization of native SK3 protein in PC12 cells.** *A*, a transmitted light image (*top*) and annular staining pattern of SK3 protein (*middle*) presumably representing membrane localization in a mock-transfected PC12 cell. Normalized fluorescent intensity histogram of SK3 fluorescence shows two sharp peaks represent the annular channel distribution (*bottom*). *B*, green fluorescent image revealing intense GFP expression in a PC12 cell transfected with IRES-GFP (*top*). Expression of GFP does not alter annular staining pattern of endogenous SK3 (*middle*), as evidenced by the intensity histogram of SK3 fluorescence (*bottom*). *C*, SK3-1C-IRES-GFP-transfected cell. GFP expression (*top*), predominantly cytosolic distribution of SK3 (*middle*), and altered SK3 fluorescence intensity histogram (*bottom*). The ratio of presumptive membrane to intracellular staining was significantly reduced in SK3-1C-IRES-GFP cells (1.42 ± 0.177, $p < 5.0 \times 10^{-7}$, one-way ANOVA) from that observed in mock and IRES-GFP-transfected cells (7.02 ± 0.860, 8.16 ± 1.09) cells.

The Dominant-inhibitory Activity of SK3-1C Is Not Due to a Nonspecific Sponge Effect on CaM Availability—Since the DIS includes part of the CaM-binding-domain (CaMBD) of SK_{Ca}/IK_{Ca} channels, and because SK3-1C exerts its suppressive effect selectively on CaM-gated channels, it is possible that SK3-1C may act as a nonselective CaM sponge. Such a mechanism has been suggested to underlie the dominant-inhibitory activity of C-terminal fragments of IKCa1 (51). To address this question, we attempted to reverse SK3-1C-mediated intracellular sequestration of endogenous SK3 protein in PC12 cells by overexpressing CaM (52) (Fig. 9*A*, *left*). PC12 cells were co-transfected with the SK3-1C-IRES-GFP and CaM plasmids at a 1:1 mass ratio, or with a bicistronic construct (CaM-IRES-SK3-1C-GFP) containing CaM and IRES-translated SK3-1C-GFP, both driven by the CMV promoter. These constructs expressed equally well and showed similar levels of GFP fluorescence (Fig. 9*A*, *middle*). Overexpression of CaM through either strategy did not reverse SK3-1C-mediated intracellular sequestration of endogenous SK3 protein in PC12 cells (Fig. 9*A*, *right*, quantitative data summarized in Fig. 9*B*).

As a further test of the nonspecific CaM sponge idea, we examined whether SK3-1C overexpression would modify Ca^{2+}-CaM-dependent inactivation of endogenous voltage-gated Ca^{2+} currents (Ca_V) in PC12 cells or the cloned L-type Ca_V channel stably expressed in HEK293T cells (53–57). SK3-1C-IRES-GFP

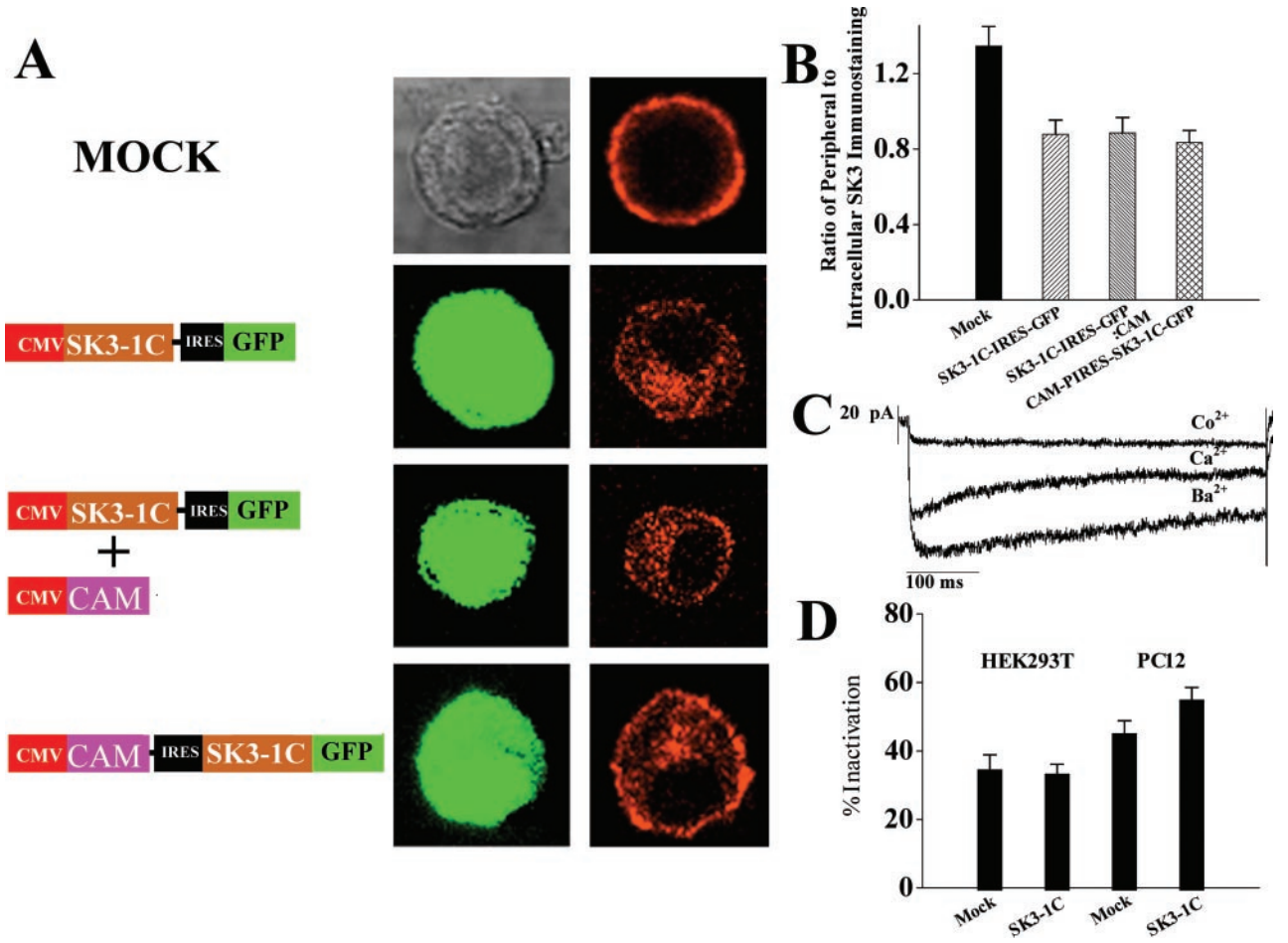

FIG. 9. **SK3-1C does not act as a nonspecific CaM sponge.** *A*, overexpression of CaM does not influence the intracellular trapping of endogenous SK3 protein in PC12 cells induced by SK3-1C expression. CaM was overexpressed along with SK3-1C using both co-transfection and a bicistronic construct (CaM-IRES-SK3-1C-GFP); constructs for this experiment are schematized on the *left* of each confocal image. The SK3-1C-GFP protein was efficiently produced by the IRES element, as evident from the comparable GFP fluorescent intensity observed following transfection of the various constructs (*middle*). SK3 localization is dramatically shifted from the cell periphery into the cytoplasm upon transfection of SK3-1C (*second panel* from the *top*), and CaM overexpression fails to reverse this phenomenon (*right*, *third* and *fourth panels* from the *top*). *B*, the peripheral to intracellular fluorescence intensity ratios of SK3 immunostaining are shown as a bar graph. No significant difference was observed between SK3-1C-transfected cells (0.878 ± 0.0761, $n = 27$), cells co-transfected with SK3-1C-IRES2-eGFP plus CaM (0.886 ± 0.0818, $p = 0.9474$, Student's t test, $n = 33$), or cells transfected with CaM-IRES-SK3-1C-GFP (0.835 ± 0.0644, $p = 0.66216$, Student's t test, $n = 33$). *C,* representative Ca_V current trace in a SK3-1C-IRES-GFP-transfected cell that stably expresses $Ca_V1.2b + \beta2a$. Ca_V currents were elicited by a depolarizing step to 30 mV. Ca^{2+}-CaM dependent inactivation is evident with 30 mM Ca^{2+} in the external solution and is absent upon substitution with 30 mM Ba^{2+}. Ca_V currents could be substantially blocked with 2 mM Co^{2+} in 30 mM Ca^{2+}. *D*, SK3-1C overexpression did not alter Ca^{2+}-CaM dependent inactivation of Ca_V currents in HEK293T cell line stably expressing $Ca_V1.2b + \beta2a$ or endogenous Ca_V currents in PC12 cells. Percent reduction in Ca_V peak current at $t = 500$ ms (% inactivation) was nearly identical in the HEK293T cell line stably expressing $Ca_V1.2b + \beta2a$ following SK3-1C-IRES-GFP transfection (32.3 ± 5.54%; $n = 7$) or mock transfection (33.8 ± 3.53%, $n = 7$). Similarly, the percent inactivation, of Ca_V currents in PC12 cells was comparable following SK3-1C-IRES-GFP-transfection (54.2 ± 7.04%, $n = 8$) or mock-transfection (44.4 ± 4.64%, $n = 8$, $p = 0.302$, Student's t test).

overexpression had no significant effect on CaM-Ca^{2+}-dependent inactivation of the cloned L-type Ca_V channel (representative trace in Fig. 9*C* and histogram in Fig. 9*D*) or the endogenous Ca_V current in PC12 cells (Fig. 9*D*), indicating that SK3-1C overexpression does not alter other CaM-mediated events. Taken together, the failure of CaM overexpression to reverse SK3-1C-mediated intracellular trapping of SK3 protein in PC12 cells and the inability of SK3-1C to alter Ca^{2+}-CaM-dependent inactivation of endogenous Ca^{2+} currents in these cells, suggests that SK3-1C does not act as a nonspecific CaM sponge.

DISCUSSION

We have identified and characterized a novel SK3 transcript, SK3-1C, that is generated by alternative utilization of a novel exon 1C instead of exon 1A used by SK3. When expressed heterologously in mammalian cells, SK3-1C suppressed whole cell K^+ currents produced by SK1, SK2, and SK3 channels, and to a lesser extent IKCa1 channels, but did not affect the iberiotoxin-sensitive BK_{Ca} channel or K_V channels. Immunolabeling and confocal microscopy studies suggested that the dominant-inhibitory activity of SK3-1C was a consequence of redistribution of SK_{Ca} proteins into intracellular compartments resulting in a decrease in the numbers of functional channels in the plasma membrane. SK3-1B also potently suppressed the entire SK_{Ca} channel family by a similar mechanism (16). Dominant-negative suppression of the family of SK_{Ca}/IK_{Ca} channels by SK3-1B and SK3-1C provides a powerful strategy to define the *in vivo* role of these channels in neuronal and non-neuronal tissues through the use of region- and tissue-specific promoters. Such an approach would have advantages over individual SK_{Ca}/IK_{Ca} gene knockouts, as evidenced by a lack of a phenotype in SK3 knockout mice (14) possibly due to compensation.

Through deletion analysis we determined that a 30-residue

domain (DIS) in the C-terminal region shared by SK3-1B and SK3-1C confers the property of negative-dominance. The DIS resembles the "tetramerizing-coiled-coiled" domain in the C termini of other K^+ channels where it contributes to tetramer stability and selectivity of multimerization (50). Since tetramerizing-coiled-coiled domains form stable tetramers (50) and the DIS is essential to the dominant-inhibitory activity of SK3-1C, DIS-dependent subunit-interactions are likely to underlie negative-dominance. Consistent with this notion, a nonfunctional SK1 mutant (hSK1YP) was recently reported to suppress SK3 channels in a dominant-negative manner by co-assembling with SK3 proteins (58). These results support a model in which non-functional isoforms of SK_{Ca}/IK_{Ca} channels regulate their functional counterparts, and consequently, the cellular functions that depend on them, by interfering with channel assembly and surface expression.

Since the DIS contains a portion of the CaMBD of SK_{Ca} channels (59), we considered the possibility that the SK3-1C-mediated dominant-inhibitory activity and intracellular sequestration of SK_{Ca} channels could result from gross disturbances of calmodulin homeostasis. However, CaM overexpression did not override SK3-1C mediated intracellular sequestration of SK3 protein in PC12 cells, and Ca^{2+}-CaM-mediated inactivation of endogenous Ca_V channels in PC12 cells was unaffected by SK3-1C overexpression. These results indicate that other CaM-mediated events are unaffected by SK3-1C overexpression, and that SK3-1C is not acting as a CaM sponge.

The high degree of sequence conservation of the DIS among members of the SK_{Ca}/IK_{Ca} family suggests that naturally occurring non-functional variants of SK1, SK2, and IKCa1 may also act as family-wide dominant-negative suppressors of SK_{Ca} channels in much the same way as do SK3-1B and SK3-1C. A search of GenBank™ revealed human SK2 transcripts (NM_170775, BC015371, BG769522) encoding truncated isoforms of the channel that may exhibit cross-channel dominant-inhibitory activity because of the presence of the DIS. Naturally occurring truncated splice variants of human SK1 have also been described (60).

Of the two dominant-negative SK3 isoforms only SK3-1B is found in the brains of humans (16), primates (BQ807391), pigs (BI341958), and cows (CB467440). SK3-1B and SK3-1C transcripts are both expressed in peripheral tissues, but SK3-1C is more abundant (Fig. 2) (16). SK3-1C mRNA levels relative to SK3-1B are particularly high in salivary gland, skeletal muscle, trachea, and lymphoid tissues. Of note is the relative abundance of SK3-1C mRNAs in the lymph node compared with the IKCa1 channel that plays a major role in regulating Ca^{2+} signaling and proliferation in lymphocytes (5, 39, 61). Selective pharmacological blockade of IKCa1 suppresses lymphocyte proliferation (61), and SK3-1C might inhibit lymphocyte activation in a similar fashion by suppression of IKCa1. Skeletal muscle and salivary gland express moderate to high levels of SK3-1C transcripts along with SK3 or IKCa1, respectively (2, 65). SK3 channels regulate the action potential threshold in denervated skeletal muscle (2) and the ratio of SK3 *versus* SK3-1B/SK3-1C in these cells might therefore finetune this process. Since the functional role of IKCa1 in the salivary gland has not been determined (65), it is hard to predict what SK3-1C will do in these cells. The molecular mechanisms responsible for the tissue-specific expression patterns of SK3-1B and SK3-1C remain to be determined.

The possible use of non-functional dominant-inhibitory subunits to regulate channel function is not unique to the SK_{Ca}/IK_{Ca} family. Non-functional isoforms of other ion channels encoded by natively expressed mRNAs (tKvLQT1/KvLQT-2, KCNQ2S, $HERG_{USO}$, HERG-1b, SloV1, Kv5.1, Kv6.1-Kv6.3, Kv8.1, Kv9.1, SK3-1B, $Ca_V1.1$, $Ca_V1.2$,) and by pathogenic mutant transcripts (KCNQ1, KCNH2, Kv1.1, $K_{ir}2.1$, SK3-Δ) have been described (7, 16, 22, 40, 42, 46–49, 61–64). Although many of these isoforms, like SK3-1C, have not been proven to exist as proteins in native tissues, they silence their functional counterparts when heterologously expressed in mammalian cells (7, 16, 22, 40, 42, 46–49, 62–64), thereby suggesting a generalized mechanism to titrate membrane excitability through variation in the levels of functional and dominant-inhibitory isoforms. Mutant truncated channel proteins with dominant-inhibitory activity underlie several channelopathies including the long QT syndrome, episodic ataxia-1, benign familial neonatal convulsion and Andersen's syndrome. Truncation mutations in KCNQ1 (KvLQT1) and KCNH2 (HERG) cause dominantly inherited forms of Long-QT syndrome via suppression of delayed rectifier K^+ channels that contribute to the repolarization phase of the cardiac action potential (47). Similar truncation mutants of Kv1.1 underlie episodic ataxia type-1 (49, 64), and truncation mutants of KCNQ2 and KCNQ3 are responsible for benign familial neonatal convulsion. Dominant-inhibitory nonfunctional mutants of $K_{ir}2.1$/KCNJ2 contribute to Andersen's syndrome, a developmental disorder with an accompanying ventricular tachycardia (48). Thus, dominant-negative suppression may be a widespread phenomenon through which the functional expression of multimeric proteins such as K^+ channels is regulated, leading to gradations in the levels of membrane excitability.

Acknowledgment—We thank Dr. Christine Beeton and Dr. Luette Forrest for useful discussions and for help in the laboratory. We thank Dr. Khaled Houammed for generously providing us with cell lines stably expressing SK1, SK2, SK3, IKCa1, Dr. Andrew Tinker for the cell line stably expressing the BK_{Ca} channel, and Dr. Franz Hoffman for donating the cell line stably expressing $Ca_V1.2b + \beta 2a$. We also thank Drs. Hans-Gunther Knaus and Martin Stocker for sharing their rodent-SK3-specific antibodies that target the C termini of these proteins, and Dr. Mitsui Ikura for providing us with the CaM clone.

REFERENCES

1. Vergara, C., Latorre, R., Marrion, N. V., and Adelman, J. P. (1998) *Curr. Opin. Neurobiol.* **8,** 321–329
2. Neelands, T. R., Herson, P. S., Jacobson, D., Adelman, J. P., and Maylie, J. (2001) *J. Physiol.* **536,** 397–407
3. Pedarzani, P., Mosbacher, J., Rivard, A., Cingolani, L. A., Oliver, D., Stocker, M., Adelman, J. P., and Fakler, B. (2001) *J. Biol. Chem.* **276,** 9762–9769
4. Wolfart, J., Neuhoff, H., Franz, O., and Roeper, J. (2001) *J. Neurosci.* **21,** 3443–3456
5. Fanger, C. M., Rauer, H., Neben, A. L., Miller, M. J., Wulff, H., Rosa, J. C., Ganellin, C. R., Chandy, K. G., and Cahalan, M. D. (2001) *J. Biol. Chem.* **276,** 12249–12456
6. Barfod, E. T., Moore, A. L., and Lidofsky, S. D. (2001) *Am. J. Physiol. Cell Physiol.* **280,** C836-C842
7. Caterrall W. A., Chandy, K. G., and Gutman, G. A. (eds), *The IUPHAR Compendium of Voltage-gated Ion Channels*, pp. 141–149, Nightingale Press, England
8. Kohler, M., Hirschberg, B., Bond, C. T., Kinzie, J. M., Marrion, N. V., Maylie, J., and Adelman, J. P. (1996) *Science* **273,** 1709–1714
9. Chandy, K. G., Fantino, E., Wittekindt, O., Kalman, K., Tong, L. L., Ho, T. H., Gutman, G. A., Crocq, M. A., Ganguli, R., Nimgaonkar, V., Morris-Rosendahl, D. J., and Gargus, J. J. (1998) *Mol. Psychiatry* **3,** 32–37
10. Ishii, T. M., Maylie, J., and Adelman, J. P. (1997) *J. Biol. Chem.* **272,** 23195–23200
11. Xia, X. M., Fakler, B., Rivard, A., Wayman, G., Johnson-Pais, T., Keen, J. E., Ishii, T., Hirschberg, B., Bond, C. T., Lutsenko, S., Maylie, J., and Adelman, J. P. (1998) *Nature* **395,** 503–507
12. Fanger, C. M., Ghanshani, S., Logsdon, N. J., Rauer, H., Kalman, K., Zhou, J., Beckingham, K., Chandy, K. G., Cahalan, M. D., and Aiyar, J. (1999) *J. Biol. Chem.* **274,** 5746–5754
13. Stocker, M., and Pedarzani, P. (2000) *Mol. Cell Neurosci.* **15,** 476–493
14. Bond, C. T., Sprengel, R., Bissonnette, J. M., Kaufmann, W. A., Pribnow, D., Neelands, T., Storck, T., Baetscher, M., Jerecic, J., Maylie, J., Knaus, H. G., Seeburg, P. H., and Adelman, J. P. (2000) *Science* **289,** 1942–1946
15. Eichler, I., Wibawa, J., Grgic, I., Knorr, A., Brakemeier, S., Pries, A. R., Hoyer, J., and Kohler, R. (2003) *Br. J. Pharmacol.* **138,** 594–601
16. Tomita, H., Shakkottai, V. G., Gutman, G. A., Sun, G., Bunney, W. E., Cahalan, M. D., Chandy, K. G., and Gargus, J. J. (2003) *Mol. Psychiatry* **8,** 524–535
17. Sailer, C. A., Hu, H., Kaufmann, W. A., Trieb, M., Schwarzer, C., Storm, J. F., and Knaus, H. G. (2002) *J. Neurosci.* **22,** 9698–9707
18. Obermair, G. J., Kaufmann, W. A., Knaus, H-G., and Flucher, B. E. (2003) *Eur. J. Neurosci.* **17,** 721–731

19. Shepard, P. D., and Bunney, B. S. (1988) *Brain Res* **463,** 380–384
20. Shepard, P. D., and Bunney, B. S. (1991) *Exp. Brain Res.* **86,** 141–150
21. Steketee, J. D., and Kalivas, P. W. (1990) *J. Pharmacol. Exp. Ther.* **254,** 711–719
22. Miller, M. J., Rauer, H., Tomita, H., Gargus, J. J., Gutman, G. A., Cahalan, M. D., and Chandy, K. G. (2001) *J. Biol. Chem.* **276,** 27753–27756
23. Bowen, T., Guy, C. A., Craddock, N., Cardno, A. G., Williams, N. M., Spurlock, G., Murphy, K. C., Jones, L. A., Gray, M., Sanders, R. D., McCarthy, G., Chandy, K. G., Fantino, E., Kalman, K., Gutman, G. A., Gargus, J. J., Williams, J., McGuffin, P., Owen, M. J., and O'Donovan, M. C. (1998) *Mol. Psychiatry* **3,** 266–269
24. Bowen, T., Williams, N., Norton, N., Spurlock, G., Wittekindt, O. H., Morris-Rosendahl, D. J., Williams, H., Brzustowicz, L., Hoogendoorn, B., Zammit, S., Jones, G., Sanders, R. D., Jones, L. A., McCarthy, G., Jones, S., Bassett, A., Cardno, A. G., Owen, M. J., and O'Donovan, M. C. (2001) *Mol. Psychiatry* **6,** 259–260
25. Cardno, A. G., Bowen, T., Guy, C. A., Jones, L. A., McCarthy, G., Williams, N. M., Murphy, K. C., Spurlock, G., Gray, M., Sanders, R. D., Craddock, N., McGuffin, P., Owen, M. J., and O'Donovan, M. C. (1999) *Biol. Psychiatry* **45,** 1592–1596
26. Dror, V., Shamir, E., Ghanshani, S., Kimhi, R., Swartz, M., Barak, Y., Weizman, R., Avivi, L., Litmanovitch, T., Fantino, E., Kalman, K., Jones, E. G., Chandy, K. G., Gargus, J. J., Gutman, G. A., and Navon, R. (1999) *Mol. Psychiatry* **4,** 254–260
27. Ritsner, M., Modai, I., Ziv, H., Amir, S., Halperin, T., Weizman, A., and Navon, R. (2002) *Biol. Psychiatry* **51,** 788–794
28. Antonarakis, S. E., Blouin, J. L., Lasseter, V. K., Gehrig, C., Radhakrishna, U., Nestadt, G., Housman, D. E., Kazazian, H. H., Kalman, K., Gutman, G., Fantino, E., Chandy, K. G., Gargus, J. J., and Pulver, A. E. (1999) *Am. J. Med. Genet.* **88,** 348–351
29. Bonnet-Brilhault, F., Laurent, C., Campion, D., Thibaut, F., Lafargue, C., Charbonnier, F., Deleuze, J. F., Menard, J. F., Jay, M., Petit, M., Frebourg, T., and Mallet, J. (1999) *Eur. J. Hum. Genet.* **7,** 247–250
30. Hawi, Z., Mynett-Johnson, L., Murphy, V., Straub, R. E., Kendler, K. S., Walsh, D., McKeon, P., and Gill, M. (1999) *Mol. Psychiatry* **4,** 488–491
31. Joober, R., Benkelfat, C., Brisebois, K., Toulouse, A., Lafreniere, R. G., Turecki, G., Lal, S., Bloom, D., Labelle, A., Lalonde, P., Fortin, D., Alda, M., Palmour, R., and Rouleau, G. A. (1999) *Am. J. Med. Genet.* **88,** 154–157
32. Chowdari, K. V., Wood, J., Ganguli, R., Gottesman, II, and Nimgaonkar, V. L. (2000) *Mol. Psychiatry* **5,** 237–238
33. Stober, G., Meyer, J., Nanda, I., Wienker, T. F., Saar, K., Jatzke, S., Schmid, M., Lesch, K. P., and Beckmann, H. (2000) *Eur. Arch. Psychiatry Clin. Neurosci.* **250,** 163–168
34. Tsai, M. T., Shaw, C. K., Hsiao, K. J., and Chen, C. H. (1999) *Mol. Psychiatry* **4,** 271–273
35. Ujike, H., Yamamoto, A., Tanaka, Y., Takehisa, Y., Takaki, M., Taked, T., Kodama, M., and Kuroda, S. (2001) *Psychiatry Res.* **101,** 203–207
36. Koronyo-Hamaoui, M., Danziger, Y., Frisch, A., Stein, D., Leor, S., Laufer, N., Carel, C., Fennig, S., Minoumi, M., Apter, A., Goldman, B., Barkai, G., Weizman, A., and Gak, E. (2002) *Mol. Psychiatry* **7,** 82–85
37. Figueroa, K. P., Chan, P., Schols, L., Tanner, C., Riess, O., Perlman. S. L., Geschwind. D. H., and Pulst, S. M. (2001) *Arch. Neurol.* **58,** 1649–1653
38. Jacobson, D., Herson, P. S., Neelands, T. R., Maylie, J., and Adelman, J. P. (2002) *Muscle Nerve* **26,** 817–822
39. Ghanshani, S., Wulff, H., Miller, M. J., Rohm, H., Neben, A., Gutman, G. A., Cahalan, M. D., and Chandy, K. G. (2000) *J. Biol. Chem.* **275,** 37137–37149
40. Smith, J. S., Iannotti, C. A., Dargis, P., Christian, E. P., and Aiyar, J. (2001) *J. Neurosci.* **21,** 1096–1103
41. Shmukler, B. E., Bond, C. T., Wilhelm, S., Bruening-Wright, A., Maylie, J., Adelman, J. P., and Alper, S. L. (2001) *Biochim. Biophys. Acta* **1518,** 36–46
42. Raghib, A., Bertaso, F., Davies, A., Page, K. M., Meir, A., Bogdanov, Y., and Dolphin, A. C. (2001) *J. Neurosci.* **21,** 8495–8504
43. Mohammad-Panah, R., Demolombe, S., Neyroud, N., Guicheney, P., Kyndt, F., van den Hoff, M., Baro, I., and Escande, D. (1999) *Am. J. Hum. Genet.* **64,** 1015–1023
44. Kupershmidt, S., Snyders, D. J., Raes, A., and Roden, D. M. (1998) *J. Biol. Chem.* **273,** 27231–27235
45. Jiang, M., Tseng-Crank, J., and Tseng, G. N. (1997) *J. Biol. Chem.* **272,** 24109–24112
46. Zarei, M. M., Zhu, N., Alioua, A., Eghbali, M., Stefani, E., and Toro, L. (2001) *J. Biol. Chem.* **276,** 16232–16239
47. Demolombe, S., Baro, I., Pereon, Y., Bliek, J., Mohammad-Panah, R., Pollard, H., Morid, S., Mannens, M., Wilde, A., Barhanin, J., Charpentier, F., and Escande, D. (1998) *J. Biol. Chem.* **273,** 6837–6843
48. Andelfinger, G., Tapper, A. R., Welch, R. C., Vanoye, C. G., George, A. L., Jr., and Benson, D. W. (2002) *Am. J. Hum. Genet.* **71,** 663–668
49. Zerr, P., Adelman, J. P., and Maylie, J. (1998) *J. Neurosci.* **18,** 2842–2848
50. Jenke, M., Sanchez, A., Monje, F., Stuhmer, W., Weseloh, R. M., and Pardo, L. A. (2003) *EMBO J.* **22,** 395–403
51. Joiner, W. J., Khanna, R., Schlichter, L. C., and Kaczmarek, L. K. (2001) *J. Biol. Chem.* **276,** 37980–37985
52. Hoeflich, K. P., and Ikura, M. (2002) *Cell* **108,** 739–742
53. Liang, H., DeMaria, C. D., Erickson, M. G., Mori, M. X., Alseikhan, B. A., and Yue, D. T. (2003) *Neuron* **39,** 951–960
54. Rane, S. G., and Pollock, J. D. (1994) *J. Neurosci. Res.* **38,** 590–598
55. Gage, M. J., Rane, S. G., Hockerman, G. H., and Smith, T. J. (2002) *Mol. Pharmacol.* **61,** 936–944
56. Peterson, B. Z., DeMaria, C. D., Adelman, J. P., and Yue, D. T. (1999) *Neuron* **22,** 549–558
57. Hohaus, A., Poteser, M., Romanin, C., Klugbauer, N. Hofmann, F., Morano, I., Haase, H., and Groschner, K. (2000) *Biochem. J.* **348,** 657–665
58. Monaghan, A. S., Benton, D. C., Bahia, P. K., Hosseini, R., Shah, Y. A., Haylett, D. G., Moss, G. W. (2003) *J. Biol. Chem.*, **279,** 1003–1009
59. Schumacher, M. A., Rivard. A. F., Bachinger. H. P., and Adelman, J. P. (2001) *Nature* **410,** 1120–1124
60. Zhang, B. M., Kohli, V., Adachi, R., Lopez, J. A., Udden, M. M., and Sullivan, R. (2001) *Biochemistry* **40,** 3189–3195
61. Wulff, H., Miller, M. J., Hansel, W., Grissmer, S., Cahalan, M. D., and Chandy, K. G. (2000) *Proc. Natl. Acad. Sci. U. S. A.* **97,** 8151–8156
62. Pereon, Y., Demolombe, S., Baro, I., Drouin, E., Charpentier, F., and Escande, D. (2000) *Am. J. Physiol. Heart Circ. Physiol.* **278,** H1908–1915
63. Crociani, O., Guasti, L., Balzi, M., Becchetti, A., Wanke, E., Olivotto, M., Wymore, R. S., and Arcangeli, A. (2003) *J. Biol. Chem.* **278,** 2947–2955
64. Adelman, J. P., Bond, C. T., Pessia, M., and Maylie, J. (1995) *Neuron* **15,** 1449–14454
65. Nehrke, K., Quinn, C. C., Begenisich, T. (2003) *Am. J. Physiol. Cell Physiol.* **284,** C535–546